Published in final edited form as:
Int J Biol Macromol. 2013 February ; 53: 42–53. doi:10.1016/j.ijbiomac.2012.10.030.

Bovine serum albumin oligomers in the E- and B-forms at low protein concentration and ionic strength

Jeremiah J. Babcock and **Lorenzo Brancaleon***
Department of Physics and Astronomy, University of Texas at San Antonio, One UTSA Circle, San Antonio, TX 78242, USA

Lorenzo Brancaleon: lorenzo.brancaleon@utsa.edu

Abstract

The manuscript describes the study of the oligomerization process of bovine serum albumin (BSA) in two different structural monomeric forms: the extended-form (E) at pH 2.0 and the basic-form (B) at pH 9.0. The study was conducted at low protein concentration (1 mg/ml) and relatively short incubation time (maximum 56 days) in order to investigate early oligomerization events rather than the formation of mature fibrils. The comparison between the two isoforms show that oligomers form much faster (~6 days) in the E-form than in the B-form where formation of oligomers requires ~4 weeks. The oligomers appear to be limited to a maximum of tetramers with size <30nm. Hydrophobic interactions from exposed neutral amino acid residues in the elongated E-form are the likely cause for the quick formation of aggregates at acidic pH. We used an array of biophysical techniques for the study and determined that oligomerization occurs without further large changes in the secondary structure of the monomers. Under the conditions adopted in this study, aggregation does not seem to exceed the formation of tetramers, even though a very small amount of much larger aggregates seem to form.

Keywords

Bovine serum albumin; Optical spectroscopy; Protein aggregation; Dynamic light scattering

1. Introduction

The study of protein aggregation has become paramount since investigations have shown that aggregated protein formations may lead, among others, to degenerative conditions like Alzheimer and Huntington disease, diabetes as well as prion disease [1,2]. The aggregation often manifests as amyloid fibrils, i.e., long, ordered fibers comprised of protein-subunits aggregated in cross-β sheet formation [3]. These fibers build up into distinct deposits identifiable with late-stage diseases, particularly Alzheimer's disease [1].The pathway of such formations is poorly understood, due to the high complexity of the conformational folding of the protein. The interactions responsible for the aggregation may include long and short-distance electrostatic potentials, disulfide/salt bridge linkage, hydrogen bonding networks and entropically-driven hydrophobic solvent-solute interactions [4]. Also unclear

*Corresponding author at: Department of Physics and Astronomy, The University of Texas at San Antonio, One UTSA Circle, San Antonio, TX 78249, USA. Tel.: +1 210 458 5694.

Appendix A. Supplementary data: Supplementary data associated with this article can be found, in the online version, at http://dx.doi.org/10.1016/j.ijbiomac.2012.10.030.

is the mechanism for changes in the secondary structure that lead to such an organized beta-rich structure.

Over the years it was discovered that many types of proteins can undergo aggregation. For instance, orderly and disorderly aggregation is widely considered to be a generic property of globular proteins [5]. Various globular proteins have shown propensity to form ordered fibrils in vitro [6–11], which suggests a common linking property for early oligomerization stages. One particular globular protein, bovine serum albumin (BSA), a well-studied blood transport protein, has been shown to form ordered and disordered fibril or spherical aggregates under various conditions [12–14]. Therefore, BSA is a good model for studying the aggregation mechanisms of globular proteins. BSA is a 585 amino acids, 66 kDa globular protein comprised of at least 67% α-helical secondary structure in physiological conditions [15]. It has three main domains which can change conformations under different conditions of pH [16,17]. The protein has 17 intramolecular disulfide links that are instrumental to keeping the compact structure, as well as a free sulfhydryl Cys34 amino residue. BSA contains two tryptophan residues Trp134 and Trp213 (Fig. 1) [18], which have been used to provide an internal indicator to inner protein solvent access and tertiary structure changes [16,19–22].

In going from acidic to basic conditions, BSA undergoes several transitions [23] which include the extended (E), fast (F), normal (N), basic (B) and aged (A) forms. For this study we focused on the E and B forms that differ greatly in overall shape and surface charges but do not introduce changes in the chemical composition. The various structures have been observed albeit with low spatial resolution [24]. The extended transition is often associated with a hydrodynamic radius increase and elongation of the molecule [25], probably led by the mobility of domain III which contribute to the loss of compactness. It was reported that a loss of as much as 40% α-helical structure was associated with the formation of the E-form [17], however, other results demonstrated a possible formation of a molten globule [26] where the protein keeps most of its secondary structure intact, but loses tertiary structure and exposes hydrophobic patches [27]. Conversely, very subtle changes occur for the N–B transition, where almost no secondary structure is lost [28], meaning the protein keeps most of its heterogeneity. A “swelling” of the tertiary structure has been observed for the protein at pH >8 [29] and attributed, in part, to changes of domain I [30].

Studies suggest that higher-order aggregation without factors like high temperature or high concentration is insignificant in the E-form [31,32], and large-scale ordered aggregate growth, such as fibrils may not be possible. Likewise, the B form does not show signs of extensive ordered aggregation without heat or denaturant [33]. Existence of a BSA dimer at pH 3.0 has been demonstrated [34], thought to be a result of inter-molecular thiol exchange. However, the time period of incubation studied previously may have been inadequate to detect non-specific aggregation events of oligomer formation in solution. In the present study we have investigated a time period in which oligomers can form without interference from larger fibrillar structures.

Chemically, the protein is the same in the B and E conformations, however its physical characteristics (i.e., shape and charge) are different. This enables us to determine purely structural and electrostatic effects on the aggregation pattern. In the work presented here we adopted a more comprehensive and fundamental approach to the early aggregation steps, using a broad array of quantitative techniques used in biophysics and material science that yield a more exhaustive characterization of the early aggregate formation.

2. Materials and methods

2.1. Material

BSA (A0281, 99% fatty acid free, Sigma–Aldrich, St. Louis, MO) was purified by dialysis at least twice at room temperature and overnight at 4°C for the acidic condition, and no purification was done for the basic condition. The buffer at pH 2 was made using sodium phosphate dihydrate at 10mM, adjusting the solution pH to 2.0 with phosphoric acid. The pH 9.0 buffer was prepared using a combination of boric acid and sodium borate also at 10mM.

In order to prevent the formation of bacteria in the solutions during the incubation time, sodium azide (0.01%), was added as antibacterial agent to both buffers. The pH of the solutions was measured periodically during the incubation period in order to ensure that it remained within 0.2 pH units of the initial value.

All BSA solutions were prepared as an initial stock at 2 mg/mL. The protein concentration was monitored with absorption spectroscopy using the molar extinction coefficient ε_{278} = 43,623 M^{-1} cm^{-1}[35]. The stocks were then diluted to a final concentration of 1 mg/mL and stored at room temperature in the dark.

2.2. Absorption spectroscopy

Absorption spectra were recorded on a dual beam Evolution 300 spectrophotometer (Thermo Fisher Scientific, Waltham, MA). The spectra were recorded from 250 nm to 750 nm, with a 1 nm resolution and 120nm/min scan speed. Baselines were recorded from the reference buffer solutions, which were also kept under the same conditions as the incubating samples. Spectral offsets due to possible variability of the instrument over time and the optical conditions of the cuvettes were removed by arbitrarily placing the zero of all spectra at 750 nm, where the protein does not absorb.

2.3. Fluorescence spectroscopy

Steady-state fluorescence spectra were recorded using an Aminco-Bowman 2 (AB2) double-monochromator fluorimeter (Thermo Fisher Scientific, Waltham, MA). The intrinsic protein fluorescence of BSA was recorded using excitation at 295 nm and emission in the 305–550 nm with a 1 nm/s scan speed and a 4nm bandwidth in both excitation and emission. Each fluorescence spectrum was the average of five consecutive scans.

2.4. Fluorescence lifetime

Lifetime decay measurements of the intrinsic protein fluorescence were taken with a Fluorocube TCSPC lifetime instrument (Horiba, Edison, NJ), utilizing a pulsed (FWHM ~700ps) 293 nm LED light source at 1 MHz repetition rate (IBH, Glasgow, UK). The monochromator excitation and emission slit widths were set at 32 nm and 12nm, respectively, to optimize the number of photon counts and ensure the proper sampling rate limit (i.e., 2.5% of the laser repetition rate). Lifetime decays were taken at the peak fluorescence wavelength of each sample, incorporating magic angle conditions to eliminate anisotropy contributions to the lifetime.

2.5. Circular dichroism spectroscopy

Circular dichroism (CD) experiments were carried out using an Olis Cary 17 dual-beam spectropolarimeter (Olis Inc., Bogart, GA). All spectra were collected in the 190–240 nm region using a 0.1 mm or 0.2 mm path length quartz cell. In order to minimize the absorption due to O_3, the instrument was thoroughly purged with N_2 collected from a liquid

nitrogen tank at 10 L/min rate. All spectra are the average of five to ten scans collected with variable integration time as a function of PMT high voltage. The background solvent CD signal was subtracted from the protein spectra to obtain the representative data. Spectra were analyzed using the CDPro spectral fitting software [36,37].

2.6. Dynamic light scattering (DLS)

Light scattering measurements were collected using a Delsa Nano C photon correlation spectrometer (Beckman-Coulter, Indianapolis, IN) with dual 30 mW 658 nm laser diodes and photomultiplier tube, fixed at 165° with a 50 μM pinhole illumination width. Data collection cycles were kept to at least 250 accumulations per cycle to increase the statistical significance of the fitted results, and at least 3 cycles were collected to ensure reproducibility of the sizing distributions. Data analysis for both cumulative and distribution sizing techniques was accomplished by assuming water solvent parameters for index of refraction and viscosity, incorporating using a NNLS (non-negative least squares) algorithm provided by the instrument software.

2.7. Atomic force microscopy

Oligomerization of the incubated BSA solution was also investigated using a Multimode V atomic force microscope (AFM) (Veeco, Santa Clara, CA) in fluid tapping mode (FTM–AFM). Samples were prepared by deposition of small aliquots of the incubated solutions on atomically flat mica sheets fixed to steel pucks. Prior to each sample deposition, the mica slides were freshly cleaved with clear tape. A volume of 30 μl of the diluted BSA solution was deposited onto the surface and left for at least 30 min. Following extensive rinsing by 0.1 μm filtered distilled water, the surface was scanned using the large-area scanner (15 μm), with Tap190-G long silicon cantilevers (FTM-AFM) (Ted Pella Inc, Redding, CA) at a resonant frequency of 190 kHz and force constant of 4N/m. The resonant frequency of the cantilever in fluid was ~35 kHz, and scans were recorded at 1 Hz, with at least a 512 line resolution. The image analysis was subsequently performed by the open-source software Gwyddion [38].

3. Data analysis

3.1. Correction of absorption spectra

As Fig. 2 shows, and as discussed more in detail in Section 4, incubation of BSA at both pH produces a decrease in the absorption spectrum and a simultaneous increase of the contribution from Rayleigh scattering [39]. A common method to correct absorption data for light scattering contributions is to analyze the double logarithmic plot of the apparent absorption vs. the wavelength in a region of the spectrum where there is no substantial contribution from the electronic transitions of the protein, i.e., >350 nm

$$\log_{10} A(\lambda) = m \log_{10} \lambda + C \quad (1)$$

A linear regression fitting provides the slope and intercept, and by taking the antilog of the data, the subtraction factor (scattering contribution) is found and removed from the spectra and linearized according to

$$A_{\text{Scatter}}(\lambda) = 10^{m \log_{10} \lambda + C} \quad (2)$$

3.2. Correction of fluorescence spectra

The corrected fluorescence intensity in arbitrary units was obtained by applying a standard correction used for elimination of potential inner filter effects [40].

$$F(\lambda)=F_0 10^{((A_{exc}(\lambda)+A_{em}(\lambda))/2)} \quad (3)$$

where A_{exc} and A_{em} are, respectively, the absorption values at the excitation wavelength and at the maximum of the emission spectrum and F_0 is the uncorrected fluorescence. The value of A_{exc} was obtained after correction for Rayleigh scattering described in the previous section, while A_{em} is the value of the emission at the fluorescence maximum.

3.3. Fluorescence lifetime

Analysis of fluorescence decay data was performed using the software DAS6.2 (Horiba, Edison, NJ). The analysis is carried out by assuming that the recorded fluorescence decay $R(t)$ is the convolution between the true fluorescence decay $I(t)$ and the instrumental response function (prompt) $G(t)$, according to the equation

$$R(t)=\int_0^t G(t-t')I(t')dt' \quad (4)$$

where $I(t)$ is of the form

$$I(t)=\sum_{i=1}^{N} a_i \exp^{-t/\tau_i} \quad (5)$$

with a_i being the pre-exponential component with lifetime τ_i. The fitting algorithm, uses the least squares method, to fit the experimental decay $R(t)$ by convoluting the experimentally recorded $G(t)$ with the theoretical function $I(t)$. The fitting minimizes the reduced χ^2 while varying a_i and τ_i. The quality of the fitting is judged by the value of χ^2, the visual inspection of the residual and the value of the Durbin–Watson factor [41] which is an indicator of the autocorrelation of the residuals. We assumed that acceptable values of χ^2 and the Durbin–Watson parameter would range between 1.0 and 1.5, and between 1.8 and 2.0, respectively. Fittings of the fluorescence decays were carried out with up to three exponential components. The fitted results were used to retrieve the average lifetime $\bar{\tau}$ [40] as

$$\langle\tau\rangle \frac{\sum_i \alpha_i \tau_i^2}{\sum_i \alpha_i \tau_i} \quad (6)$$

The fractional contribution, f_i, to the steady-state intensity can be found further using

$$f_i=\frac{\alpha_i}{\sum_i \alpha_i} \quad (7)$$

3.4. Circular dichroism

The spectral output has been calculated in mean residue ellipticity (MRE)

$$[\theta]_\lambda = \frac{M_w \theta_\lambda}{10\,(N-1)\,dc} \quad (8)$$

where M_w is the molecular weight of the protein in Daltons, θ_λ is the measured ellipticity (degrees), N is the number of residues, d is the cell path length (cm), and c(g/L) is the concentration of the protein. For BSA, the molecular weight is 66,463 Da, with 585 residues [18]. Two approaches were used to analyze the spectra: spectral fitting with CDPro [36,37] and analysis of the helical content using the method of Greenfield and Fasman [42] that employed the following two empirical equations:

$$(\%\alpha - \text{helix}) = \left[\frac{[\vartheta]_{202} - 4000}{-33,000 - 4000}\right] \times 100 \quad (9A)$$

$$(\%\alpha - \text{helix}) = \left[\frac{[\vartheta]_{222} - 3000}{-36,000 - 3000}\right] \times 100 \quad (9B)$$

The fitting analysis with CDPro provides several different basis sets and algorithms that can yield widely different results. Spectral fitting was initially performed by comparing the three algorithms CDSSTR [43], CONTINLL [44] and SELCON3 [45]. Each algorithm provides various basis sets, each composed of a varying number of proteins with relatively similar structures. After several trials the CDSSTR algorithm with the SP43 and SDP48 basis set was selected. The basis sets represent an ensamble of forty three globular soluble proteins without (SP43) and with (SDP48) five denatured proteins. Fitting of each CD spectrum in the 190–240 nm region, was therefore carried out with each of the two basis sets and the results were thereby averaged. This provides a measure of the uncertainty in determining each structure.

4. Results

The two different pH incubation conditions were selected because BSA assumes two different conformations at these two values: the compact B-Form (pH 9) and the elongated E-Form (pH 2) [23]. The incubation time was selected to investigate the period (lag time) where the protein has not formed mature fibrils and is undergoing oligomerization events. The results have been presented first in terms of aggregation dynamics in order to establish the existence of oligomer states, and then the spectroscopic data have been reviewed in order to follow the protein structural dynamics up to the aggregation events.

4.1. Aggregate sizing

4.1.1. Dynamic light scattering—DLS was used to detect changes in the hydrodynamic radius of the protein and the formation of its aggregates in solution as a function of incubation. Table 1 shows the results of the DLS measurements of the BSA incubated in both conditions. The cumulative hydrodynamic diameters over the incubation period show that at acidic pH, larger-scale aggregation begins by the fourth day, therefore indicating a relatively fast aggregation kinetics. The polydispersion indices, a measure of the distribution of measured particle sizes, seem to increase in the same time period, demonstrating that multiple-sized protein particles exist in solution. This becomes evident when looking at the volume-weighed differential intensity distributions of the protein in solution in Fig. 3A. Immediately evident is the primary peak around 10–20 nm, which increases slightly over the time of incubation. Other larger peaks become evident at later time points. These peaks can be separated into two groups: protein aggregates below 200 nm in diameter and large

agglomerates whose cause is not clear at the moment but is neglected in our discussion since we are only interested in smaller aggregates. The overwhelming contributor to the scattering intensity is the primary peak below 30 nm, which indicates that the protein exists in a stable configuration, most likely a low-order oligomer. Furthermore, the increase in hydrodynamic diameter as shown in Table 1 may not be due to an increase in the size of the stable conformation, but instead to the increased contributions pertaining to the mid-range aggregates below 200 nm and the large agglomerates in solution.

The measurements at pH 9 require a longer time frame of incubation (~8 weeks). The volume-weighed distributions for BSA aggregates have been shown in Fig. 3B. Again, a primary peak in the 10–20 nm range can be seen throughout the 8 weeks of incubation. This indicates that the protein exists in a stable configuration.

Unlike the peak at pH 2 (E-form) that shows only a slight shift to larger sizes, the peak center at basic pH (B-form) shifts to larger hydrodynamic radii by week 6. Also, at this pH, large aggregates and agglomerates are present from the beginning of the run. Some mid-range aggregates do build up over time, but their relative contribution to the scattering intensity is small, pointing to their instability.

Although it is difficult to quantify the oligomeric state from the primary peak, it offers an indication of size spread and relative contributions.

4.1.2. Atomic force microscopy (AFM)—Atomic force microscopy was incorporated to complement the sizing results for DLS. Unlike DLS, AFM has the capability to resolve particle topology. In the AFM studies of the aggregating protein, two time points (6 days for the E-form at acidic pH and 28 days for the B-form at basic pH) were chosen from the DLS and UV–VIS absorption data (Figs. 2 and 3A and B) that indicated the likely occurrence of oligomerization. In both cases, the AFM measurements were taken to determine whether oligomerization or fibrillation had occurred in either condition. No elongated fibrils were found at either pH in this time period.

Representative results of AFM on BSA aggregates for pH 2 and 9 have been shown in Fig. 4A and B, where each image has been corrected for tip shape effects by model tip fitting. The aggregation pattern shown by the protein in acidic conditions can be visualized in Fig. 4A, as taken from the final incubated state at 6 days, and in Fig. 4B, showing the alkaline solvent-incubated proteins at 4 weeks. After applying appropriate grain threshold fitting, the statistical quantities to include average diameter, height and grain volume of both images were found and have been summarized in Table 2. In fact, the distributions obtained from grain fitting can be seen in Fig. 4C and D, which represent, respectively, the height (*Z*-axis) distributions of the particles, and the distribution of the particle size. In both cases, the grain sizes were obtained by area fitting by an equivalent disk radius (EDR) [46].

It is clear from the results that the aggregation of serum albumin in pH 2 conditions was more organized than at the pH 9 conditions. The average E-form aggregate was found to be 30.2 nm in diameter by 10.9 nm in height (Table 2), with an approximate oligomer size of 3–4, with the assumption that the hydrated volume of the protein of 262 nm^3[24] did not appreciably change upon combination with a like-hydrated protein in the aggregation process. The size distribution of Fig. 4D enabled us to determine that the most likely size of the aggregates in the E-form was 10.1 nm. The distribution also shows that the average size was skewed to the more largely spherical aggregates observable (Fig. 4A), but the overall size of the protein aggregates was commensurate with the results of DLS, where the modal distributions reported that the majority of the proteins existed in sizes less than 20 nm.

Furthermore, although difficult to observe from Fig. 4A, the small-scale (less than 20 nm) particles are not spherical in nature, but more elongated and irregular in dimensions.

Looking at the results of the B-form in Fig. 4B, the dominant size of particle seems to be small. In fact, the grain fitting (Table 2) shows the average size of the particles as 11.6nm in diameter by 7.3 nm in height (after 4 weeks of incubation), a marked difference from the aggregates in pH 2 conditions (6 incubation days). This agrees with the most likely size of the particles of 10.6 nm obtained from Fig. 4D, and also with the DLS modal distribution of 9.3 nm at this time period. The oligomer state from the grain fitting was estimated to be smaller than a hexamer, again assuming the hydrated volume of $188nm^3$[47] remained constant upon combination of the monomers.

4.1.3. Optical spectroscopy—From the sizing studies presented earlier, the extent of aggregation in both conditions was not extensive, as the most likely protein combination with dimensions in the range of 10–20nm is small oligomers with less than 5–6 monomers per aggregate. Furthermore, it was found that no fibrils had been formed at the end of either time period. The steady-state spectral data were recorded in order to establish secondary and/or tertiary conformational changes in BSA during the oligomerization process.

4.1.4. Absorption spectroscopy—Fig 2A and B show the spectra of BSA in solution over an observation period of 8 weeks for the alkaline solution and 6 days for the acidic solution. The signature aromatic absorption peak at 280 nm can be seen in both cases with varied trends. For the pH 2 solution (Fig. 2A), there is a slight blue-shift from the original spectra but overall no intensity decrease over time which could be indicative of disulfide bond oxidation or aromatic quenching. Furthermore, beyond the absorption band (>310nm), no evidence of substantial light scattering became relevant, which would account for increased aggregation in solution. From the sizing data presented earlier, it was clear that short-time-scale aggregation did occur for the E-form of BSA, but the absence of light scattering reinforces the data found in the volume-distributed scattering data from DLS (Fig. 3A) where small scale aggregates <~100nm were prevalent. However, it should be noted that the noise of the pH 2 absorption spectra is considerably larger than that at pH 9 (compare Fig. 2A and B). Thus, more subtle scattering changes for $\lambda > 300$ nm may be more difficult to detect. Considering that the incident wavelength in the non-absorbing region (>310 nm) is an order of magnitude larger than the diameter of the aggregates (Table 1), Rayleigh scattering conditions were in effect, where the scattering intensity can be considered proportional to the sixth power of the particle diameter in solution [39].

$$I(\lambda,\theta)=I_0\frac{1+\cos^2(\theta)}{2R^2}\left(\frac{2\pi}{\lambda}\right)\left(\frac{n^2-1}{n^2+1}\right)\left(\frac{d}{2}\right)^6 \quad (10)$$

On the other hand, there was a small trend of intensity decrease in the pH 9 absorption band (Fig. 2B) accompanied by a slight increase in scattering above 310 nm, indicating a larger population of scattering particles indicative of particle aggregates. Based on the DLS results (Fig. 3 and Table 1) we attribute this increase to the small number of large aggregates that appear in solution over time.

4.1.5. Fluorescence spectroscopy—Fluorescence spectroscopy can probe the environment of the tryptophan (Trp) residues in BSA and can be used for studying folding/unfolding and aggregation [16]. Changes in fluorescence intensity or wavelength emissions maxima indicate changes in the local environment of the Trp. Such changes are evident by comparing the non-incubated samples for the E- and B-forms (Fig. 5A and B). The fluorescence maximum is blue-shifted (λ_{max} = 325 nm) at the acidic pH compared to the

one at pH 9 (λ_{max} = 336nm). This difference has already been documented [23,48] and is due to the fact that despite the elongated form, the Trp residues find themselves in a less polar environment due to proto-nation of proximal residues and inclusion in hydrophobic pockets [16]. Confirmation of this comes from measurement done at the same pH with N-acetyl-tryptophanamide (NATA) that do not show any substantial shift of the emission maximum between pH 9 and pH 2 thus ruling out an effect of the pH on the indole emission maximum (not shown).

The BSA fluorescence, upon incubation at pH 2, changes over time (Fig. 5A). After an initial decrease (first day), the emission intensity seemed to rise over the course of the experiment before starting to plateau after the fourth day. At the same time, the wavelength of the emission peak shifted to shorter wavelengths by ~6 nm.

The spectra of BSA in pH 9 solutions over 8 weeks (Fig. 5B) do not follow the same trend. The fluorescence intensities of the proteins decrease almost linearly over the experimental time, while keeping a relatively constant emission peak at λ_{max} = 336 nm. At week 4 there is a small blue-shift (~2 nm).

4.1.6. Lifetime fluorescence decay—The information given by fluorescence spectroscopy can be enhanced by the inclusion of fluorescence lifetime decay. An increase or decrease in fluorescence lifetime can again indicate local environmental factors surrounding the Trp residues [49]. Therefore, the intrinsic tryptophan lifetime decay data was collected incorporating fitting of the fluorescence lifetime decays with the multi-exponential model of Eq. (5). For both conditions, a two-exponential fit was found to be adequate. The results of lifetime decay fitting for both pH 2 and pH 9 conditions for the incubated BSA can be viewed in Table 3.

At pH 2, the average lifetime $\langle \tau \rangle$, found by Eq. (6), remains nearly constant throughout the incubation, as viewed in Fig. 6A. There was an approximate difference of 180 ps from the initial 3.68 ns measured, through the maximal lifetime measured at the third day at 3.86 ns to the final value of 3.79 ns. The fractional contributions to the steady-state fluorescence of the two lifetime components, calculated from Eq. (7), also remain virtually constant to a 30:70% ratio throughout the experiment.

The initial lifetime decay measured for pH 9, as seen in Table 3, was 1.76 ns longer than the one at pH 2 consistent with a different conformation of the B-form compared to the E-form. The average lifetime decreased over time, almost 490 ps, shown in Fig. 6B. Compared to the decay at pH 2, the ratio of the fractional contributions to the steady-state intensity does not remain constant but instead changed from an 18:82% to a 23:77% ratio. This indicates that, if the lifetime differences can be attributed to dynamic structural changes like aggregation, some changes in relative contributions have occurred, something not evident in the E-form.

4.1.7. Circular dichroism spectroscopy (CD)—In order to gain better understanding of the structural identity of BSA during incubation, CD was performed in the far UV (190–240 nm) as described in Section 2. The characteristic troughs at 208 nm and 222 nm of a α-helical protein (Fig. 7) can be seen, throughout the entire incubation period indicating that the main helical propensity of BSA is not affected in the time period of the incubation. However, in agreement with previous reports [16] the results show a difference in the α-helical nature of BSA between the two conditions. Analysis of the CD spectra of non-incubated samples with CDPro (Table 1 in supplemental material) and the Greenfield–Fasman equations (Table 4), shows a decrease of helical content from ~67% at pH 9 and pH 7 to 50% at pH 2.

From Fig. 7A and B, it is clear that slight spectral changes did occur at both pH values as a function of incubation. Spectral fitting with CDPro at both pH, fails to detect significant changes in the secondary structure (Table S1, supplemental material). First of all only the CDSSTR algorithm using the chosen SP43 and SDP48 bases found a composition that reproduces the structural content expected from native human serum albumin crystal structure [50] (i.e., ~67% α-helix), whereas all the other algorithm failed. This algorithm, however, fails to detect changes in the secondary structure as a function of incubation time (aggregation). This is likely due to limitations of the algorithm [36,51] as well as the fact that the structural changes might be at the limit of the detection of the computational algorithm. The result is that CDPro fitting only shows large fluctuations in the secondary structure composition (Table S1 in supplemental materials) due, in part, to the rigid limits of the spectral range that fail to properly fit the spectra (Fig. S1A and B in supplemental materials). On the other hand an analysis with the Greenfield–Fasman equation shows separate trends for incubation at the two pH values. At acidic pH incubation from day 0 to days 6 seems to produce a slight increase (from 49% up to 55%) in the helical content that is verified at both $[\theta]_{208}$ and $[\theta]_{222}$. Conversely, at pH 9 the incubation, albeit on a much longer time scale, shows a decrease in the helical content from 67% at day 0 to 61% at week 8. These changes are small but could be significant in the development of the aggregates.

5. Discussion/conclusion

Throughout the course of the experiments on the BSA early aggregation process at acidic and basic pH, two different aspects have been analyzed: (i) the relation between structural data and the aggregate sizes (using DLS and AFM), and (ii) the effects on the secondary and tertiary structure (followed using optical spectroscopy). Compared to other studies, rapid protein aggregate buildup into fibrils was not a desired effect of the current investigation, which focuses instead on the mechanism of formation of early protein oligomers. The rate limiting process chosen to inhibit any fast aggregation mechanisms included the choice of low ionic strengths for the buffer solutions, and relatively low protein concentration.

The increased optical absorption at the tail of the aromatic region (300–320 nm) of Fig. 2B for pH 9 is consistent with the presence of large aggregates in solution. The DLS results for both the E and B forms showed a unimodal distribution of sizes consistent with small scale oligomers. For both conditions the modal peak was narrow and consistently less than 30 nm (Fig. 3). DLS suggests that even though larger-scale aggregates do exist in solution, their relative concentration is small compared to the modal peaks over the time period that we have investigated.

AFM did show a representative distribution of particles images in aqueous solution. By using known hydrated volumes of the extended and basic forms, we established through grain fitting that the average particles size was consistent with dimers of BSA at pH 9, and tetramers at pH 2. The contribution of larger aggregates was very limited, in good agreement with the DLS data. For the low ionic strength buffers used in the experiment, and the relatively low concentration of the protein (1 mg/ml), the random collision rate was therefore not enough to form nucleation for larger aggregates. Some additional energy (e.g., heat) is needed to facilitate the growth phase in these conditions.

On the other hand, we have demonstrated that the light scattering contribution increases over time (Fig. 2B) for pH 9, but does not appreciably increase for the pH 2 solution. The data collected from DLS/AFM suggests an increased concentration of smaller multimers that produce a larger scattering signal in agreement with previous results [49,51]. Recalling that the average size of particle yielded by AFM experiments was 30nm ×10.9nm for pH 2 and its distribution was largely skewed toward smaller particles (Fig. 4D), the overwhelming

contribution to the scattering intensity would be the small oligomers that do not substantially affect the UV absorption and/or fluorescence spectra. The presence of scattering in the pH 9 solution is likely due to the presence of few larger agglomerates (and possibly impurities) that built up over the much larger incubation time required by alkaline pH. DLS data confirms this interpretation since the only substantial effects are seen on very large aggregates rather than on oligomers.

The inherent difficulty with identification of the oligomeric states of the protein in the two conditions, especially with DLS, comes from the lack of knowledge of the packing arrangement of the associated proteins. This is illustrated, albeit crudely, by Fig. 8, where some possible oligomer configurations and the resulting hydrodynamic diameters associated with each configuration have been represented. Since the hydrated form of the protein resembles a prolate ellipsoid with 3.5:1 axial ratio for the native form [52], 6.5:1 [47] for the basic form, and 9:1 [53] for the elongated form, the structures more consistent with the AFM results will be those most resembling a sphere. As Fig. 8 shows, the difference between hydro-dynamic diameters is limited, ranging roughly to a little more than a factor of two comparing the tetramer and monomer. In a scattering intensity distribution, the resolution of multimeric aggregates by hydrodynamic radius is not so straight-forward, due to the demonstrated diversity of protein configurations when aggregating together.

Böhme et al. [54] demonstrated that the hydrated albumin had a hydrodynamic diameter of 18.6 ± 1.2 nm for the E-form, and 12.0 ± 0.4 for the B-form. This is qualitatively in agreement with what was shown by Atmeh et al. [47] where even larger oligomers were considered. Comparing these results to ours in Figs. 3 and 4, it is evident that at least tetramer sized oligomers exist for pH 2 and possibly pH 9, albeit formed over two very different time scales (days vs. weeks). In order to gain a suitable answer to the state of oligomers for the two conditions, size-exclusion chromatography methods like HPLC or SDS-PAGE electrophoresis could be used in further studies (but are not currently available to us). However, for the purposes of this study, it is sufficient to state that both solution conditions primarily are comprised of small-scale oligomers.

More importantly, it becomes instructive to find the spectral components of the presumed small-scale oligomers and infer their local interactions. In the case of the extended form (pH 2) of BSA, it was shown that the fluorescence intensity initially decreases, then steadily increases while blue-shifting (Fig. 5A). On the other hand the value of $\langle \tau \rangle$ (Table 3) showed little change. The data in non-incubated samples is consistent with what has been seen in the past [16]. The blue-shift of the E-form is due to the insertion of at least one of the two Trp residues into a more hydrophobic environment and/or the neutralization of some residues at this low pH [16]. Although there is no crystal structure resolved for BSA, the homology with human albumin, whose crystal structure has been resolved [15] has led to assume that Trp134 and Trp213 (incidentally this position is identical in bovine and human albumin) are located in subdomain IA and between subdomain IB and IIA respectively [55]. The initial decrease in intensity is likely due to an initial partial unfolding that is followed by the formation of oligomers. These oligomers are likely formed via the interaction among hydrophobic pockets left exposed by the E-form of the protein that overcome the excess of positive charge on the protein at acidic pH. Their formation shields the Trp residues producing the increased emission intensity as well as the increase in the value of $\langle \tau \rangle$ [56].

Evidence of the mechanisms of the small-scale aggregation process can be further seen by analyzing the CD data. Over the time of incubation at pH 2 the content of the helical component increases with the formation of the small scale aggregates. This could signify that the aggregation process shields patches of hydrophobic residues, previously exposed by the extended conformation, and trigger a partial refolding of the protein. An alternative

analysis is the one yielded by Greenfield and Hitchcock-DeGregori [57] whereby a change in the CD ratio $[\vartheta]_{222}/[\vartheta]_{202}$ indicates the presence of coiled helices. This ratio decreases at pH 2 over the time of incubation (Table S2, supplemental material). This could indicate that the partial restoring of helical content at pH 2 "relaxes" coiled helices that may have twisted as a mechanism to partially shield hydrophobic residues in the non-aggregated E-form. Since the aggregation kinetics was not extensive for this time period, and the topological data obtained from the AFM showed the formation of globular or disk-like aggregates the initial steps identified in this study may not be sufficient to start the formation of fibrils without the simultaneous introduction of other parameters, such as higher temperature, that provide enough energy to form the structured fibrils seen by incubating the protein at higher temperature.

The data at pH 9 propose a different mechanism at alkaline pH. Fluorescence intensity and lifetime decay decreased over the 8 weeks incubation (Fig. 5B, Table 3). This indicates a change in the local environment of the Trp residues, consistent with previous findings [56].

The emission blue-shift associated with the large decrease in intensity, as seen by the pH 9 condition, is consistent with the formation of aggregates in which the Trp residues get further shielded from the aqueous solvent and at the same time is quenched by the proximity of strong fluorescence quenching groups of other residues, such as one of the 17 free Cys residues and/or the carbonyl residues of the peptide bond [22,58,59]. Viallet et al. [60] attributed the major contributor of BSA fluorescence to Trp134, which is located near the surface of subdomain IA [55]. It is therefore plausible to assume that this region of the protein is involved in monomer-to-monomer contact producing the quenching of the Trp residue through the quenching mechanism described above for the pH 9 condition and that oligomerization brings a quenching group (e.g., a free Cys residue, the carbonyl group of peptide bond, etc.) in proximity of this residue as proposed for other quenching mechanisms for albumins [16]. At pH 9, however the analysis with the Greenfield–Fasman equation shows a decrease of helical conformation, indicating that the formation of small aggregates over the time of incubation starts to decrease the helical content of the proteins. On the other hand the $[\vartheta]_{222}/[\vartheta[_{202}$ ratio (Table S2) increases at alkaline pH, indicating that the formation of aggregates in the already extensively helical B-form may induce some winding of helices in contact with each other in the aggregate.

6. Conclusion

Our experiments were directed at understanding early aggregation mechanisms in albumin at two very different conformations: the E-form (pH 2) and the B-form (pH 9). We propose several conclusions:

1. Early aggregation of BSA proceeds much faster at acidic pH than at basic pH. Whereas the E-form produces aggregates in the time scale of less than 1 week, the B-form requires several weeks (>6) to form aggregates of similar size;
2. Such a different aggregation kinetics can be explained by the fact that the extended E-form, despite being positively charged, leaves several large hydrophobic areas exposed to the solvent. As a result two or more E-form monomers aggregate through hydrophobic interaction that overcomes the electrostatic repulsion. The B-form instead remains relatively compact and the electrostatic repulsion cannot be overcome by hydrophobic interaction since the hydrophobic areas remain by-and-large shielded from the aqueous solvent;
3. Aggregates formed in this time period at both pH values are predominantly oligomers and there is no evidence of substantial formation of fibrillar aggregates;

4. There are only minor changes in the secondary conformation of the protein during the early aggregation process (a small gain of helical conformation by the acidic aggregates and a slight loss of helical content by the alkaline aggregates) and within the time frame of our experiment we did not detect structural changes that hinted at the formation of beta-aggregates (such as amyloid formation)

Although our results show the clear indication of a difference oligomerization pattern at the two pH values, future experiments will try to clarify the details of the steps that lead to the oligomerization. A combination of additional experimental techniques (e.g., size exclusion chromatography) and computational methods (e.g., molecular dynamic simulations) will be attempted to clarify the aspects of early oligomerization of albumin under alkaline and acidic conditions.

Supplementary Material

Refer to Web version on PubMed Central for supplementary material.

Acknowledgments

This work was in part funded by grant No. 2G12RR013646-11 from the Research Centers in Minority Institutions of the National Center for Research Resources, NIH (to LB.). We would also like to thank Dr. Drew Johnson, Department of Civil and Environmental Engineering, for the use of the DelsaNano dynamic light scattering system.

References

1. Dobson CM. Trends in Biochemical Sciences. 1999; 24:329–332. [PubMed: 10470028]
2. Chiti F, Dobson CM. Annual Review of Biochemistry. 2006; 75:333–336.
3. Nelson R, Sawaya MR, Balbirnie M, Madsen AØ, Riekel C, Grothe R, Eisenberg D. Nature. 2005; 435:773–778. [PubMed: 15944695]
4. Wang SS, Wu JW, Yamamoto S, Liu HS. Biotechnology Journal. 2008; 3:165–192. [PubMed: 18034432]
5. Krebs MRH, Domike KR, Donald AM. Biochemical Society Transactions. 2009; 37:682–686. [PubMed: 19614575]
6. Goldschmidt L, Teng PK, Riek R, Eisenberg D. Proceedings of the National Academy of Sciences. 2010; 107:3487–3492.
7. Maurstad G, Prass M, Serpell LC, Sikorski P. European Biophysics Journal. 2009; 38:1135–1140. [PubMed: 19688345]
8. Giurleo JT, He X, Talaga DS. Journal of Molecular Biology. 2008; 381:1332–1348. [PubMed: 18590743]
9. Taboada P, Barbosa S, Castro E, Mosquera V. Journal of Physical Chemistry B. 2006; 110:20733–20736.
10. Fändrich M, Fletcher MA, Dobson CM. Nature. 2001; 410:165–166. [PubMed: 11242064]
11. Xu M, Ermolenkov VV, He W, Uversky VN, Fredriksen L, Lednev IK. Biopolymers. 2005; 79:58–61. [PubMed: 15962278]
12. Bhattacharya M, Jain N, Mukhopadhyay S. Journal of Physical Chemistry B. 2011; 115:4195–4205.
13. Vetri V, Librizzi F, Leone M, Militello V. European Biophysics Journal. 2007; 36:717–725. [PubMed: 17624524]
14. Veerman C, Sagis LMC, Heck J, van der Linden E. International Journal of Biological Macromolecules. 2003; 31:139–146. [PubMed: 12568921]
15. Carter D, Ho J. Advances in Protein Chemistry. 1994; 45:153–203. [PubMed: 8154369]
16. Dockal M, Carter DC, Ruecker F. Journal of Biological Chemistry. 2000; 275:3042–3050. [PubMed: 10652284]

17. El Kadi N, Taulier N, Le Huerou JY, Gindre M, Urbach W, Nwigwe I, Kahn PC, Waks M. Biophysics Journal. 2006; 91:3397–3404.
18. Peters TJ. Advances in Protein Chemistry. 1985; 37:161–245. [PubMed: 3904348]
19. Chen RF. Biochimicaet Biophysica Acta. 1966; 120:169–171.
20. Cowgill RW. Biochimicaet Biophysica Acta. 1963; 75:272–273.
21. Cowgill RW. Biochimicaet Biophysica Acta. 1967; 140:37–44.
22. Cowgill RW. Biochimicaet Biophysica Acta. 1968; 168:431–438.
23. Foster, JF. Albumin Structure, Function and Uses. Pergamon Press; New York: 1977.
24. Champagne M, Luzzati V, Nicolaieff A. Journal of the American Chemical Society. 1958; 80:1002–1003.
25. Bendedouch D, Chen S. Journal of Physical Chemistry. 1983; 87:1473–1477.
26. Muzammil S, Kumar Y, Tayyab S. European Journal of Biochemistry. 1999; 266:26–32. [PubMed: 10542047]
27. Christensen H, Pain RH. European Biophysics Journal. 1991; 19:221–229. [PubMed: 2060495]
28. Leonard WJ Jr, Vijai KK, Foster J. Journal of Biological Chemistry. 1962; 238:1984–1988. [PubMed: 13929708]
29. Sen P, Ahmad B, Khan R. European Biophysics Journal. 2008; 37:1303–1308. [PubMed: 18463861]
30. Ahmad B, Kamal MZ, Khan RH. Protein and Peptide Letters. 2004; 11:307–315. [PubMed: 15327362]
31. Ikeda S, Nishinari K. Biomacromolecules. 2000; 1:757–763. [PubMed: 11710208]
32. Reichmann ME, Charlwood PA. Canadian Journal of Chemistry. 1954; 32:1092–1099.
33. Vetri V, D'Amico M, Foderà V, Leone M, Ponzoni A, Sberveglieri G, Militello V. Archives of Biochemistry and Biophysics. 2011; 508:13–24. [PubMed: 21303653]
34. Williams EJ, Foster JF. Journal of the American Chemical Society. 1960; 82:3741–3745.
35. Gill SC, von Hippel PH. Analytical Biochemistry. 1989; 182:319–326. [PubMed: 2610349]
36. Sreerama N, Woody RW. Analytical Biochemistry. 2000; 287:252–260. [PubMed: 11112271]
37. Sreerama N, Woody RW. Methods in Enzymology. 2004; 383:318–351. [PubMed: 15063656]
38. Necas D, Klapetek P. Central European Journal of Physics. 2012; 10:181–188.
39. Timasheff SN. Journal of Colloid and Interface Science. 1966; 21:489–497.
40. Lakowicz, JR. Principles of Fluorescence Spectroscopy. third. Springer; New York: 2006.
41. Durbin J, Watson GS. Biometrika. 1951; 38:159–178. [PubMed: 14848121]
42. Greenfield N, Fasman GD. Biochemistry. 1969; 8:4108–4116. [PubMed: 5346390]
43. Johnson WCJ. Proteins: Structure Function and Genetics. 1999; 35:307–312.
44. Provencher SW, Glockner J. Biochemistry. 1981; 20:33–37. [PubMed: 7470476]
45. Sreerama N, Woody RW. Analytical Biochemistry. 2003; 209:32–44. [PubMed: 8465960]
46. Klapetek P, Valtr M, Necas D, Salyk O, Dzik P. Nanoscale Research Letters. 2011; 6:514. [PubMed: 21878120]
47. Atmeh R, Arafa I, Al-Khateeb M. Jordan Journal of Chemistry. 2007; 2:169–182.
48. Brewer JM, DeSa RJ, Wampler JE. Biochemical and Biophysical Research Communications. 1977; 76:572–578. [PubMed: 1027448]
49. Vivian JT, Callis PR. Biophysical Journal. 2001; 80:2093–2109. [PubMed: 11325713]
50. Carter DC, He XM, Munson SH, Twigg PD, Gernert KM, Broom MB, Miller TY. Science. 1989; 244:1195–1198. [PubMed: 2727704]
51. Bobba A, Cavatorta P, Attimonelli M, Riccio P, Masotti L, Quagliariello E. Protein Sequences & Data Analysis. 1990; 3:7–10. [PubMed: 2315300]
52. Squire PG, Moser P, O'Konski CT. Biochemistry. 1968; 7:4261–4272. [PubMed: 5750167]
53. Harrington WF, Johnson P, Ottewill RH. Biochemical Journal. 1956; 62:569–582. [PubMed: 13315216]
54. Böhme U, Scheler U. Chemical Physics Letters. 2007; 435:342–345.

55. Bhattacharya M, Jain N, Bhasne K, Kumari V, Mukhopadhyay S. Journal of Fluorescence. 2011; 21:1083–1090. [PubMed: 21128099]

56. Qiu W, Zhang L, Okobiah O, Yang Y, Wang L, Zhong D, Zewail AH. Journal of Physical Chemistry B. 2006; 110:10540–10549.

57. Greenfield NJ, Hitchcock-DeGregori SE. Protein Science. 1993; 2:1263–1273. [PubMed: 8401212]

58. Chen Y, Liu B, Yu HT, Barkley MD. Journal of the American Chemical Society. 1996; 118:9271–9278.

59. Froehlich PM, Nelson K. Journal of Physical Chemistry. 1978; 82:2401–2403.

60. Viallet PM, Vo-Dinh T, Ribou AC, Vigo J, Salmon JM. Journal of Protein Chemistry. 2000; 19:431–439. [PubMed: 11195967]

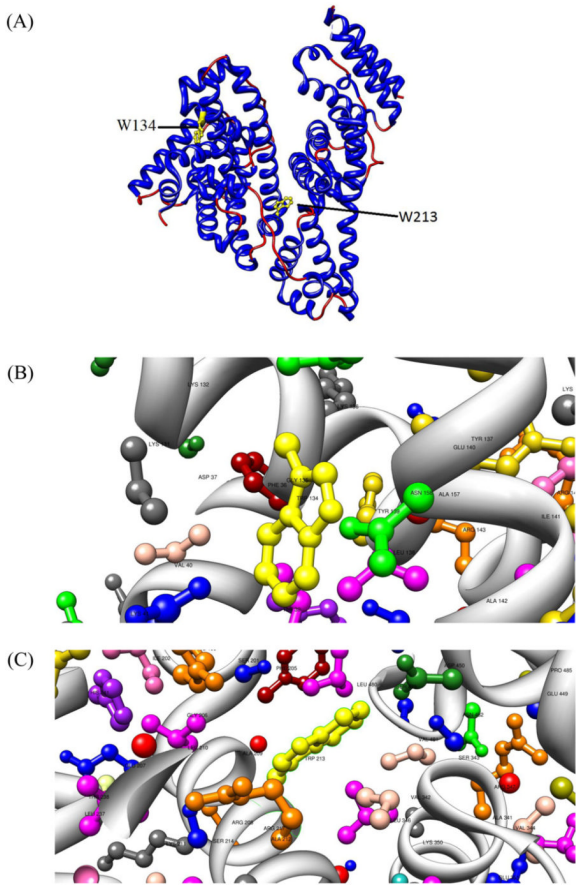

Fig. 1.
(A) Ribbon representation of the homology structure of BSA. The two Trp residues at position 134 and 213 are highlighted. Trp134 is positioned within domain I while Trp213 is located at the bottom of the central cleft of the heart-shaped protein. (B) Amino acid residues proximal to Trp134. (C) Amino acid residues proximal to Trp213.

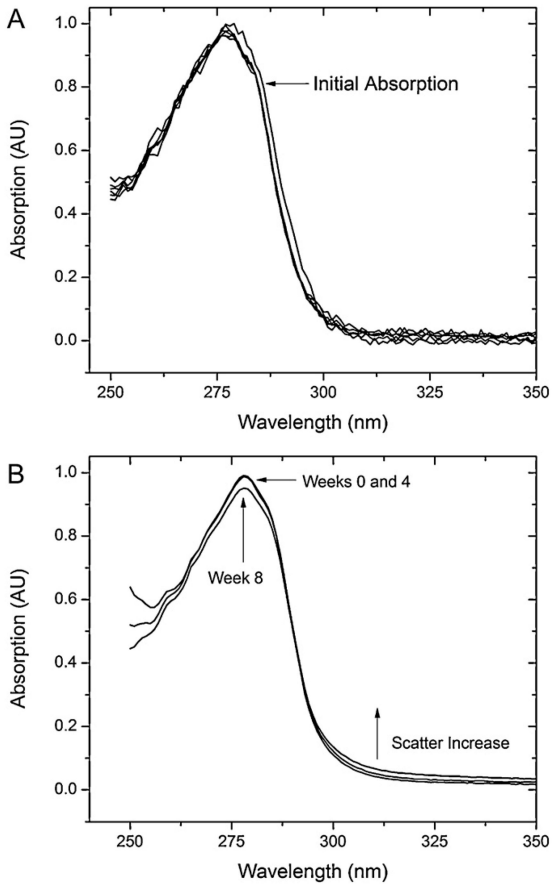

Fig. 2.

Normalized UV–Vis absorption spectra of BSA samples at different incubation times for (A) pH 2.0 buffer and (B) pH 9.0 buffer. The time of observation is indicated by the number with arrows pointing to the corresponding spectrum. In (A) the initial (Day 0) absorption spectrum is indicated by the arrow, followed by the inclusion of the remaining spectra spanning the days of the experiment. No significant change can be seen. In (B) only three spectra have been presented, the initial (the number zero corresponds to the initial reading), 4th week and final week (eighth). Normalization was applied to each set of conditions, not the overall collection, so the actual measured optical density of the two conditions did differ, indicating different concentrations.

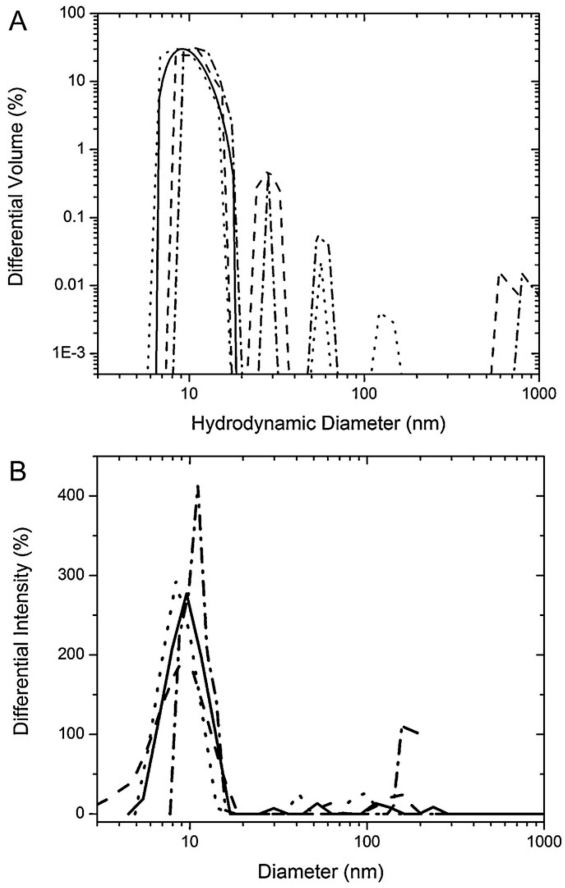

Fig. 3.

Overlay volume distribution of differential light scattering intensity found utilizing the NNLS fitting algorithm for both conditions. The hydrodynamic radii peaks show the relative size and intensity contribution to the overall scattering spectrum. The size cutoff has been selected at 1000 nm to preclude any large agglomerates, which cannot be the target protein oligomers. (A) For BSA in pH 2 solution, the size distributions have been shown in multiples of 2 day increments, starting with the initial reading day 0 (—), day 2 (– –), day 4 (···) and day 6 (– · –). The data has been represented in a log-log format with the lower limit set above zero to avoid discontinuities. (B) BSA pH 9 solution size distributions have been represented by 2 week increments up to the 4th week, where it was assumed small-scale oligomerization had been completed: Week 0 (—), Week 2 (– –), Week 4 (···) and Week 8 (– · –). The final measurement at the 8th week has been added to show the extent of these small oligomer contributions to the overall sizing. The larger aggregate contributions are not negligible in comparison to the modal peak, so a semi-log plot was chosen.

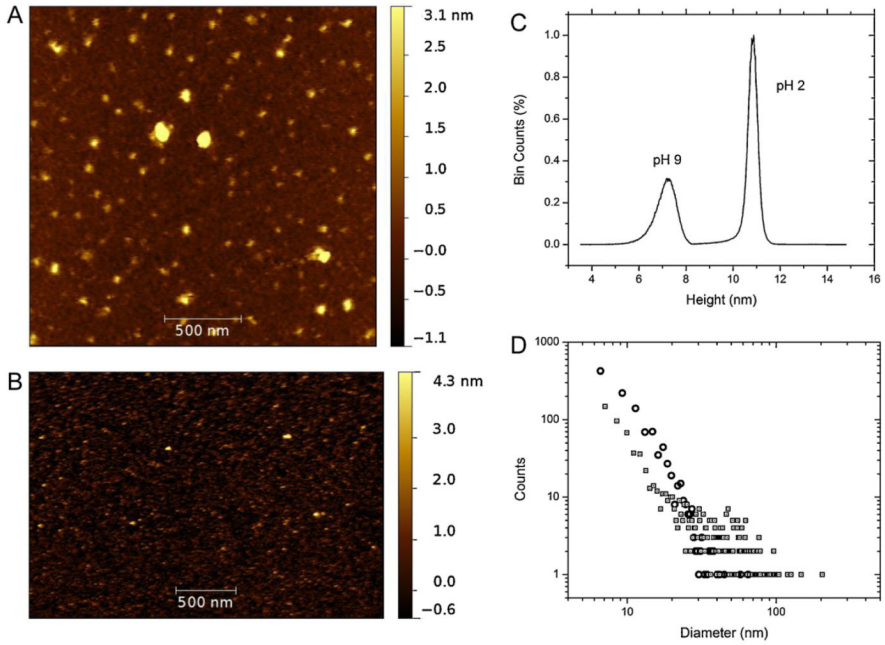

Fig. 4.

AFM imaging results for (A) pH 2 and (B) pH 9 solutions of BSA captured with FTM–AFM on cleaved mica. The scan sizes were not the same so the image resolution differs. The height distributions for both conditions are shown in (C) where the two have been combined and marked with text to distinguish between the two. The relative percentage of counts are shown in % bin counts. The equivalent disk diameters, found by threshold grain fitting of both images, representing the size of a disk large enough to cover the surface area of a particle, is shown in (D). The data has been presented in a log–log format to view the varied numbers of particles for both conditions, which were different for each image. The hollow circles represent pH 9, while the hollow squares with dots in the center represent pH 2.

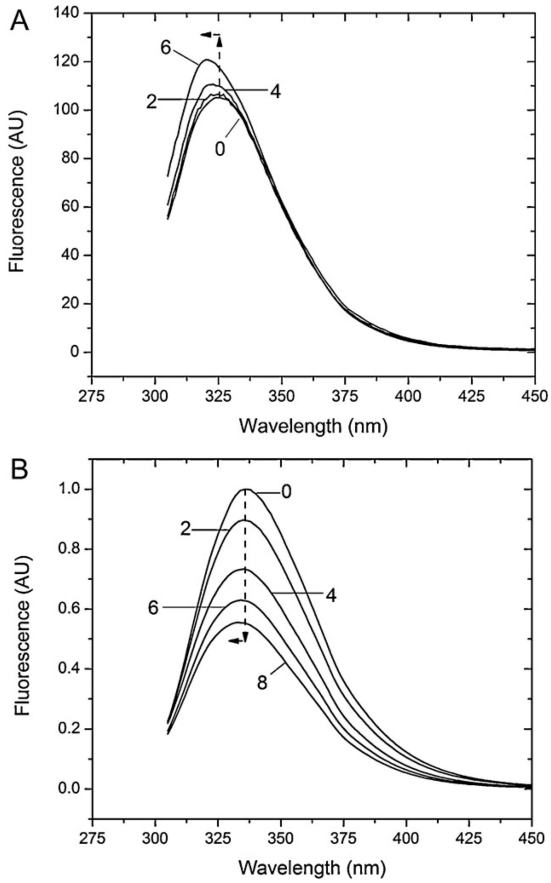

Fig. 5.

In (A) the steady state spectra of BSA at pH 2 have been presented in two days intervals, zero being the initial spectrum. The spectra show the increase of the fluorescence over the incubation time and the shift of the maximum to shorter wavelengths. In (B) the steady state spectra of BSA at pH 9 have been presented in 2 week intervals with labeling week times, zero being the initial spectra. The dotted arrows at the fluorescence peaks provide a reference to the initial week 0 peak maximum, and show the trend downward and to the left of the spectra over time. In the figure, the integrated, inner-filter effect corrected (Eq. (3)) peak intensity has been shown to preclude intensity drops as a function of peak wavelength, as such changed over the course of the experiment.

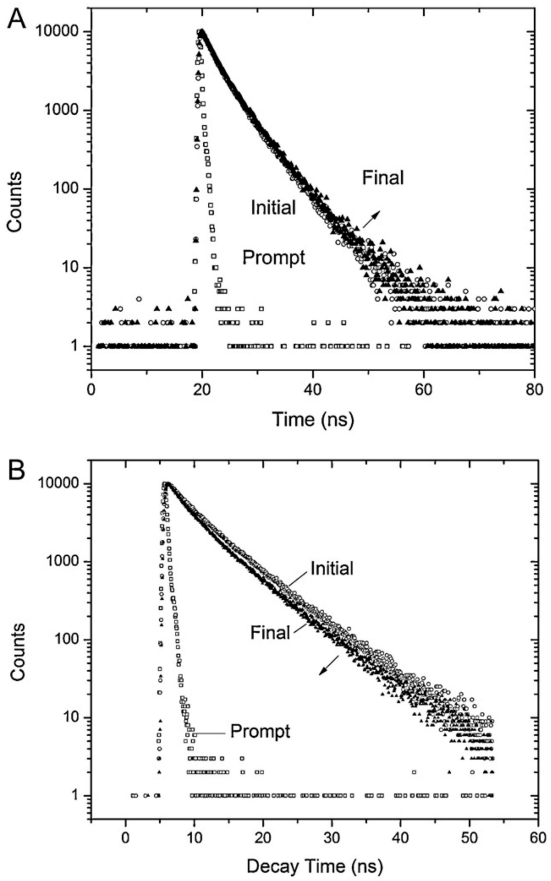

Fig. 6.

Lifetime decay peak measurements of (A) pH 2 and (B) pH 9 with channel widths of 50 or 100 ns and maximum count of 10,000. The initial and final readings, corresponding to the first (solid triangle – day 0) to the final (blank circle) measurements representing 6 days forpH 2 and 8 weeks forpH9 are shown to illustrate the relative change of lifetime decay over the experimental time. The arrow indicates the direction of decay change overtime. The prompt (blank square) is shown to provide a visual on the FWHM pulse time of the LED source.

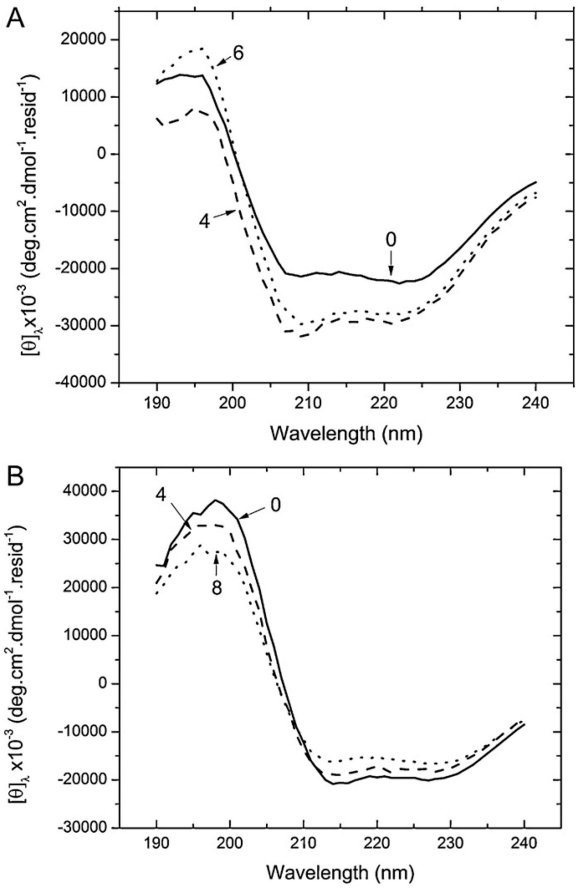

Fig. 7.

Circular dichroism spectra obtained from the solutions of BSA in (A) pH 2 solution. The spectra represent the initial (—), 4th day (– –) and 6th (···) day readings. The spectra has been represented in mean residue ellipticity. Labels have been placed to point out the corresponding spectra. (B) contains the spectra for pH 9 solutions of BSA. Here the data has been shown in MRE as the initial (—), 4th week (– –)and final 8th week (···) results to best show when the differences in aggregation time frames.

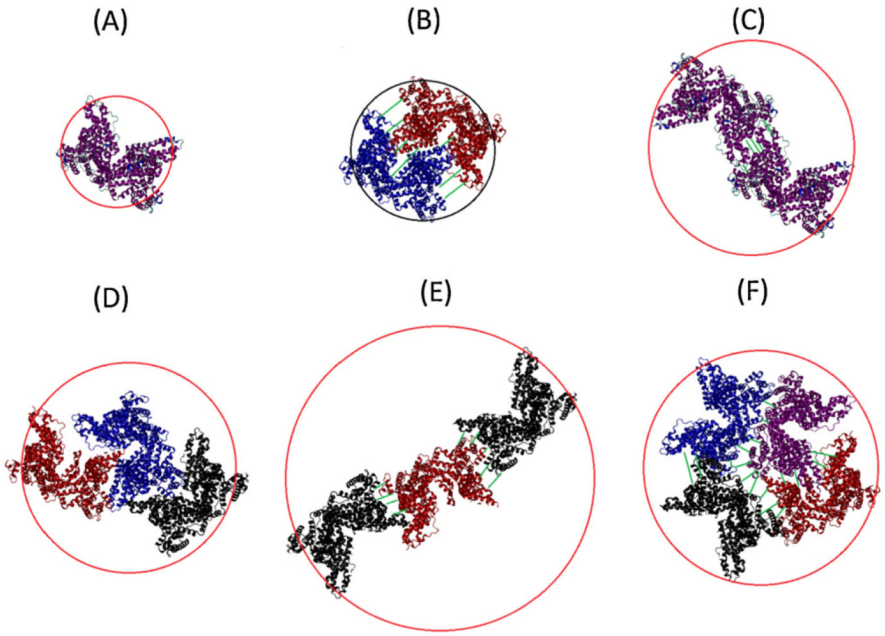

Fig. 8.

Rough visualization of possible configuration of bovine serum albumin oligomers, circled by the effective hydrodynamic diameter. The visualizations incorporate the crystal structure of HSA, which is assumed to resemble the structure of BSA. (A) monomer form, (B) dimer form fitted side to side, (C) dimer form fitted end-to-end, (D) trimers form with close association, (E) trimer formation end-to-end and (F) tightly packed tetramer form. The different colored proteins represent different subunits of the oligomer.

Table 1

Cumulant and modal hydrodynamic diameters obtained from volume-based differential light intensity distributions. The polydispersity index (PDI) shows the relative spread of particle sizes for the cumulant diameter, an average taken from cumulant fitting. The smaller the PDI, the more monodisperse the size population is.

	Modal diameter[a] (nm)	Cumulant diameter[b] (nm)	Polydispersity index
pH 2 (days)			
0	13.1 ± 1.9	16.2 ± 3.13	0.108 ± 0.014
1	12.0 ± 1.9	17.7 ± 1.21	0.341 ± 0.010
2	12.7 ± 2.4	38.8 ± 4.74	0.215 ± 0.008
3	11.4 ± 1.9	20.2 ± 1.40	0.289 ± 0.015
4	11.3 ± 2.5	279 ± 22.1	0.154 ± 0.004
5	14.9 ± 3.7	194 ± 11.0	0.216 ± 0.002
6	12.8 ± 2.6	70.3 ± 14.9	0.217 ± 0.014
pH 9 (weeks)			
0	10.3 ± 3.5	278.1	0.152
1	12.2 ± 3.6	257.3	0.353
2	9.3 ± 3.8	344.7	0.181
4	9.3 ± 3.2	157	0.171
5	11.0 ± 3.7	363.1	0.211
6	10.6 ± 4.0	372.9	0.208
7	9.3 ± 2.8	140.8	0.187

[a]The modal diameter is the most populated size, otherwise measured as the peak of the differential intensity distribution.

[b]Cumulant diameters found from fitting the autocorrelation function.

Table 2

Grain statistics taken from threshold fitting.[a]

BSA condition	Mean diameter (nm)	Mean height (nm)	Mean volume (nm^3)	Mean oligomer state
pH 2	30.2 ± 6.0	10.9 ± 1.2	852	~3–4
pH 9	11.6 ± 5.6	7.3 ± 0.7	204	~1–2

[a]The hydrated volume of a single monomer was assumed to be ~188 nm^3 for the basic form [47], while the volume of an extended form monomer was taken to be 262 nm^3, as found by [24].

Table 3

Fitting results of fluorescence decay spectra (λ_{exc} = 295 nm, λ_{em} = 330 ± 6 nm).

	Fractional contributions (%)		Individual fitted lifetimes (ns)		Average lifetime (ns)
	f_1	f_2	τ_1	τ_2	$\langle\tau\rangle$
pH 2					
Initial	30.0 ± 0.01	70.0 ± 0.02	1.49 ± 0.049	4.62 ± 0.017	3.68 ± 0.012
Day 1	29.4 ± 0.02	70.6 ± 0.03	1.61 ± 0.063	4.74 ± 0.037	3.82 ± 0.013
Day 2	29.9 ± 0.01	70.1 ± 0.02	1.63 ± 0.070	4.75 ± 0.029	3.82 ± 0.013
Day 3	29.4 ± 0.01	70.6 ± 0.01	1.62 ± 0.024	4.80 ± 0.010	3.86 ± 0.012
Day 4	29.8 ± 0.03	70.2 ± 0.03	1.60 ± 0.030	4.74 ± 0.024	3.80 ± 0.008
Day 5	29.5 ± 0.05	70.5 ± 0.05	1.58 ± 0.012	4.72 ± 0.020	3.79 ± 0.011
Day 6	30.0 ± 0.02	70.0 ± 0.02	1.58 ± 0.011	4.73 ± 0.026	3.79 ± 0.011
pH 9					
Initial	0.18 ± 0.01	0.82 ± 0.01	2.01 ±0.18	6.14 ± 0.10	5.42 ± 0.14
Week 1	0.18 ± 0.01	0.82 ± 0.01	1.76 ± 0.17	5.99 ± 0.13	5.26 ± 0.15
Week 2	0.19 ± 0.01	0.81 ± 0.01	1.77 ± 0.01	5.87 ± 0.15	5.10 ± 0.09
Week 3	0.20 ± 0.02	0.81 ± 0.02	1.83 ± 0.11	5.96 ±0.14	5.16 ± 0.17
Week 4	0.19 ± 0.01	0.81 ± 0.01	1.70 ± 0.10	5.87 ± 0.15	5.10 ± 0.18
Week 5	0.21 ± 0.02	0.80 ± 0.02	1.72 ± 0.13	5.85 ± 0.16	5.02 ± 0.20
Week 7	0.22 ± 0.02	0.78 ± 0.02	1.74 ± 0.13	5.88 ± 0.15	5.00 ± 0.20
Week 8	0.23 ± 0.03	0.77 ± 0.03	1.72 ± 0.13	5.83 ± 0.16	4.91 ± 0.20

Int J Biol Macromol. Author manuscript; available in PMC 2014 February 01.

Table 4

Relative contribution of α-helix in incubated samples as obtained by Eq. (9A).

	pH 2		**pH 9**
Initial reading	49%	Initial reading	67%
Day 1	51%	Week 1	65%
Day 2	50%	Week 2	64%
Day 3	54%	Week 3	66%
Day 4	54%	Week 4	65%
Day 5	55%	Week 5	65%
Day 6	53%	Week 6	63%
		Week 7	61%
		Week 8	60%